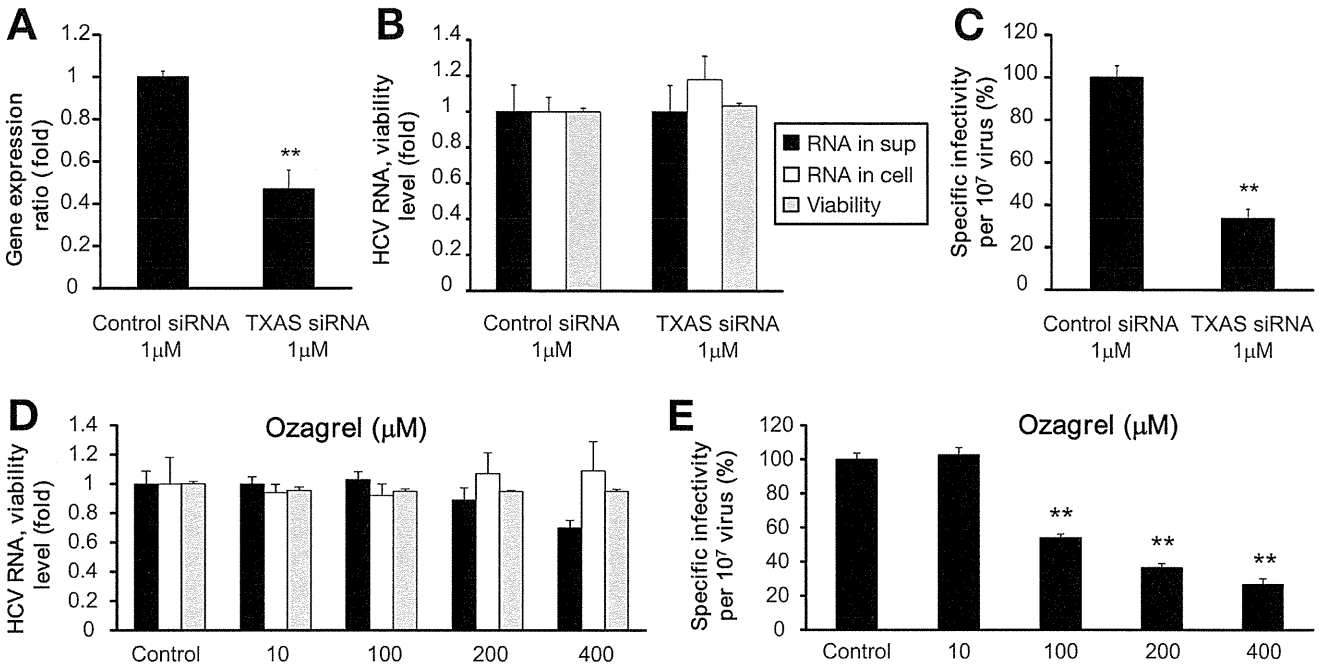


**Figure 3.** Effect of TXAS on infectious HCV production. (*A*) siRNA-mediated knockdown of TXAS mRNA expression. (*B*) Effects of TXAS-specific siRNA on HCV-RNA levels in the HCVcc-producing cell-culture system. (*C*) Effects of control and TXAS-specific siRNA on the infectivity of HCVcc in medium obtained from HCVcc-producing cell cultures were assessed. (*D*) Effects of Ozagrel on HCV-RNA levels were assessed in HCVcc-producing cell cultures. (*E*) Effects of Ozagrel on the infectivity of HCVcc produced from the cell-culture system were assessed. **Differs from control, $P < .001$.

### *$TXA_2$ Receptor Is Not Required for TXAS-Dependent Regulation of Infectious HCV Production*

$TXA_2$ exerts its physiologic functions through the $TXA_2$ receptor (TP) on plasma membranes.[17] To examine the contribution of $TXA_2$/TP signaling, we investigated the effects of the TP agonist U-46619 in our system. Regardless of dose, however, U-46619 did not affect infectious HCVcc production in the culture system (Supplementary Figure 7). Treating Huh-7-derived cell lines with the TP agonist did not increase the calcium ion concentration—a major downstream effect of $TXA_2$/TP signaling—even though the activity of U-46619 was confirmed in HEK293 cells[17] (Supplementary Figure 8*A*). We also evaluated the activity of U-46619 in terms of TP-dependent activation of Rho and observed the Rho-dependent stress fiber formation induced with U-46619 in HEK293 cells (Supplementary Figure 8*B*). In addition,

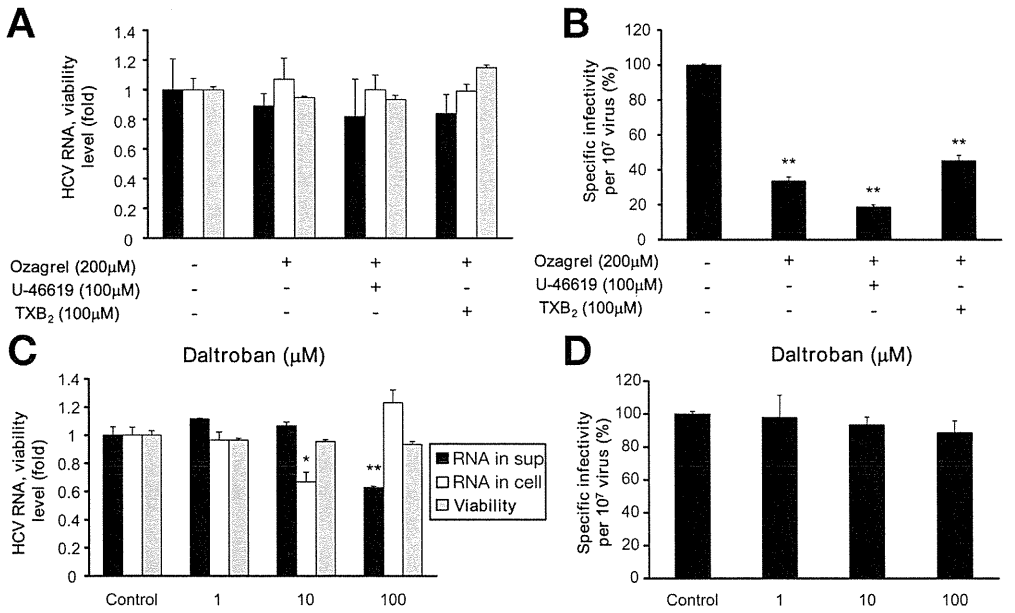


**Figure 4.** Role of TP in infectious HCVcc-producing cell cultures. (*A*) Effects of U-46619 and $TXB_2$ on HCV-RNA levels in HCVcc-producing cell cultures in the presence of Ozagrel were assessed. (*B*) The infectivity of HCVcc in culture medium from HCVcc-producing cells treated with U-46619 or $TXB_2$ in the presence of Ozagrel was assessed. (*C*) Effect of daltroban on HCV-RNA levels in HCVcc-producing cell cultures. (*D*) The infectivity of HCVcc in culture medium from HCVcc-producing cells treated with daltroban. *Differs from control, $P < .01$; **differs from control, $P < .001$.

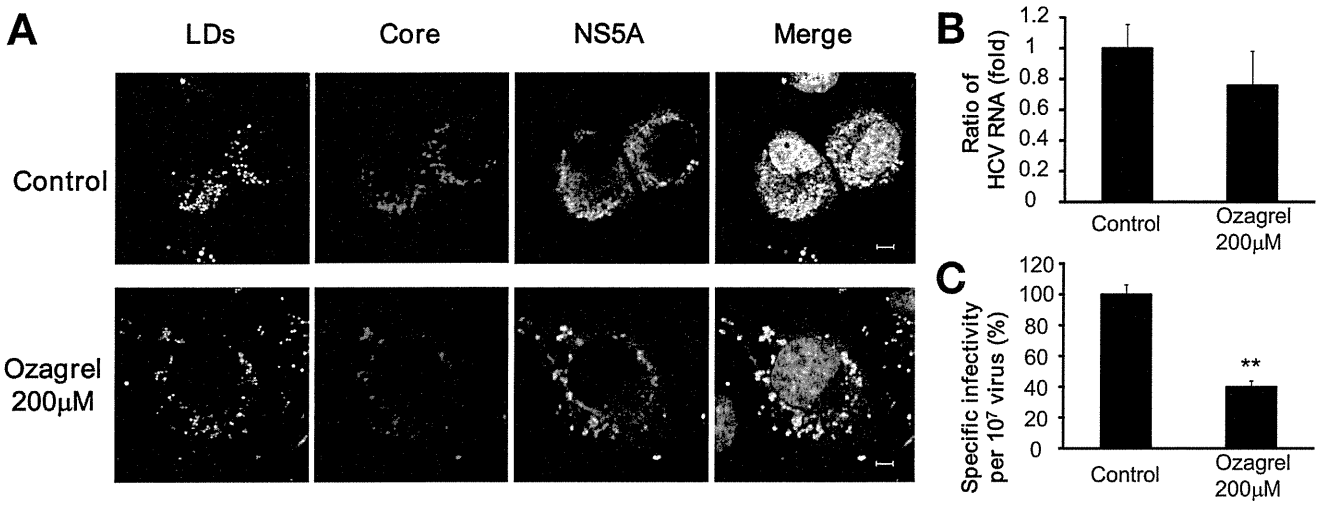


**Figure 5.** Core and NS5A near LDs and the quantity and infectivity of intracellular HCVcc. (*A*) HCV core (magenta) and NS5A (cyan) around LDs (yellow) in HCVcc-producing cells treated with the indicated reagents were observed using immunofluorescence analysis. Nuclei were stained with 4′,6-diamidino-2-phenylindole (gray). Scale bars, 5 μm. (*B*) Levels of intracellular HCV RNA obtained from the cells treated with Ozagrel. (*C*) The infectivity of intracellular HCV from cells treated with Ozagrel. Averages of triplicate samples from 2 independent experiments ± SD are shown. **Differs from control, $P < .001$.

the level of TP mRNA was, if any, quite low in human hepatocyte-derived cells and primary human hepatocytes, although only a small amount of the mRNA was detected in HuS-E/2 cells (Supplementary Figure 3*B*). These data suggest that $TXA_2$/TP signal transduction is deficient in Huh-7-derived cell lines.

To determine whether TP on the Huh-7 cells was saturated with endogenous $TXA_2$ ligand, we examined the effects of U-46619 in the presence of Ozagrel. U-46619, however, did not rescue the Ozagrel-mediated suppression of infectious HCVcc production (Figure 4*A* and *B*). In addition, the TP antagonist daltroban did not affect infectious HCVcc production (Figure 4*C* and *D*). These data indicate that TP-mediated signaling is not involved in TXAS-dependent regulation of infectious HCVcc production. In addition, we examined whether $TXB_2$—a stable metabolite of $TXA_2$ that does not activate TP—could be used to replace TXAS during infectious HCVcc production. $TXB_2$ did not counteract the effects of Ozagrel (Figure 4*A* and *B*), and did not by itself affect the HCV lifecycle (Supplementary Figure 7). These data suggest that $TXA_2$ or an unidentified metabolite of $TXA_2$ acts as a TP-independent regulator of infectious HCV production (see Discussion section).

### *TXAS-Derived Signaling Contributes to HCV Infectivity*

A previous study showed that infectious HCV is produced near LDs, to which HCV proteins are recruited.[6] As shown in Figure 5*A*, inhibiting TXAS did not markedly affect the locations of the viral proteins core and NS5A around LDs, suggesting that TXAS-derived signaling does not contribute to the recruitment of HCV proteins to the LDs. Next, to examine whether TXAS-mediated signaling drives the egression of infectious HCVcc from the cells, we analyzed intracellular HCVcc in cells treated with Ozagrel. Levels of intracellular HCVcc RNA in Huh-7 cells treated with or without Ozagrel were equivalent (Figure 5*B*). Nevertheless, the infectivity of intracellular HCVcc from the cells treated with Ozagrel was decreased markedly, as was that of HCVcc in the medium (Figure 5*C*). This result indicated that TXAS-derived signaling is not involved in the release of infectious HCV particles. Taken together, it seems likely that TXAS-derived signaling plays a role in infectious particle formation in the cells.

### *Inhibition of TXAS Changes the Physicochemical Properties of HCVcc*

We next analyzed HCVcc produced from cells treated with Ozagrel using sucrose density gradient ultracentrifugation. As reported previously,[11] 2 types of fractions containing either highly infectious, low-density HCVcc (peak fraction, 6) or less infectious, high-density HCVcc (peak fraction, 5) were obtained using samples derived from cells without treatment with Ozagrel, indicating that infectious HCVcc was present mainly in fraction 6 (Figure 6, white bars, upper and lower panels). On the other hand, analyzing Ozagrel-treated cells showed decreased levels of HCV RNA in fraction 6 (Figure 6, solid lines, upper and lower panels). Of note, the amount of HCV RNA in fraction 5 remained similar with or without Ozagrel treatment (Figure 6, lower panel). These results suggest that inhibition of TXAS-mediated signaling changes the physicochemical characteristics of HCVcc, resulting in altered infectivity.

### *A TXAS Inhibitor and IP Agonists Inhibit Early HCV Expansion in bbHCV-Infected Chimeric Mice*

Finally, we examined the in vivo anti-HCV effects of a TXAS inhibitor using bbHCV and urokinase plasminogen activator/severe combined immunodeficiency mice bearing transplanted human hepatocytes. The IP

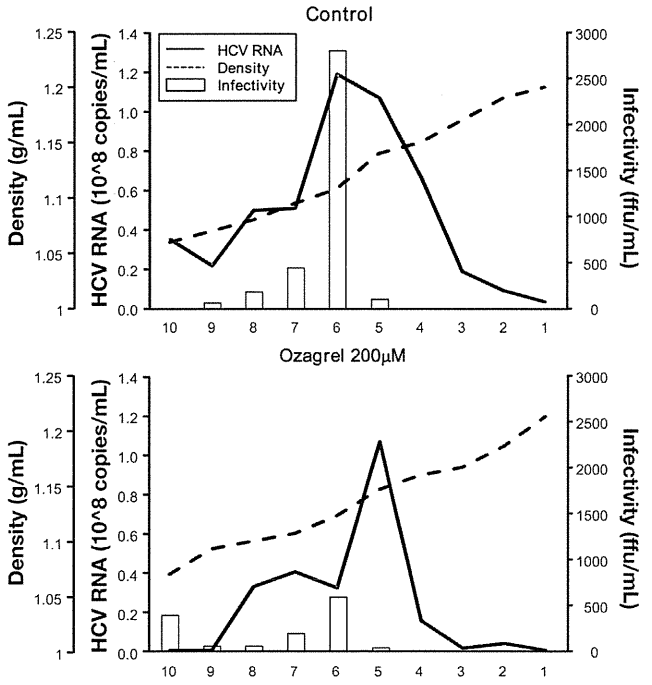


**Figure 6.** Buoyant density of HCVcc produced from cells treated with Ozagrel. *Lower* and *upper panels* show the results of HCVcc from the cells with and without Ozagrel treatment, respectively. HCV RNA (*solid line*), fraction density (*dotted line*), and HCV infectivity (*white bars*) in each fraction collected after ultracentrifugation are shown. Representative results from 2 independent experiments are shown.

agonist Beraprost also was tested because $PGI_2$ produces effects opposite of $TXA_2$ during several physiologic processes, including vascular constriction in human beings.[25] Both drugs delayed the increase in serum levels of HCV RNA (Figure 7). Of note, even 4 weeks after treatment, Beraprost reduced serum HCV-RNA levels to less than a quarter of those observed in control mice (Figure 7). Our results indicate that these drugs may inhibit HCV proliferation in vivo, and that inhibition of TXAS-derived signaling and activation of IP-mediated $PGI_2$ signaling can control HCV proliferation. Although we examined the effects of the PGIS and IP agonist on the HCV lifecycle using the HCVcc-producing cell-culture system, Beraprost did not result in any notable changes (Supplementary Figure 9). To examine whether the Huh-7 cells respond to the IP agonist, we assessed cAMP signaling using a plasmid-bearing cAMP-responsive element in a promoter upstream of the luciferase gene; cAMP signaling is a major intracellular signaling pathway that is activated by IP agonists. The IP agonist, however, did not activate cAMP signaling in Huh-7 cells even though the pathway was activated in HuS-E/2 cells.

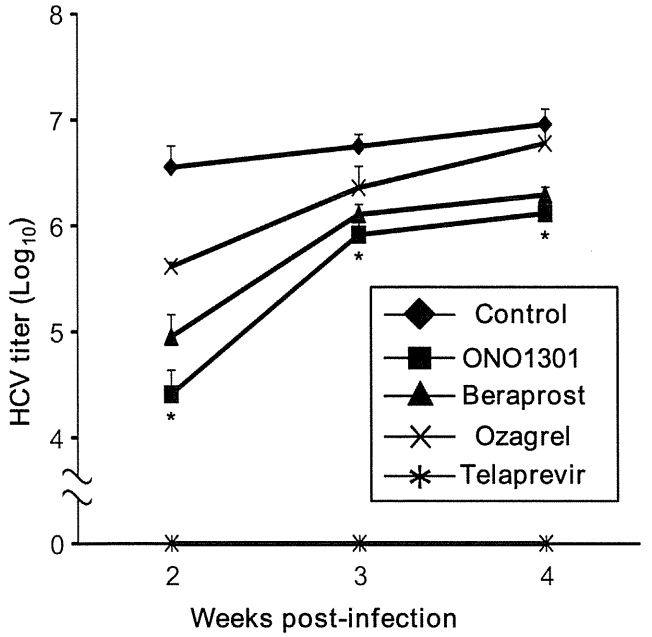


**Figure 7.** Effects of ONO1301, Beraprost, Ozagrel, and Telaprevir on the expansion of bbHCV-infected urokinase plasminogen activator/severe combined immunodeficiency mice bearing human hepatocytes. Data are presented as means ± SD for 6 (control, *diamonds*), 4 (ONO1301, *squares*; Ozagrel, *crosses*; Telaprevir, *asterisk*), and 3 (Beraprost, *triangles*) samples. *Differs from control, $P < .05$.

As another candidate anti-HCV drug, we examined the effect of ONO1301, possessing both TXAS-inhibitor and IP-agonist activities, in the humanized chimeric mouse. ONO1301 produced the most robust suppression of HCV infections (Figure 7). The effects of ONO1301 also were studied in the HCVcc-producing cell cultures, as with Ozagrel. ONO1301 suppressed infectious HCV production (Supplementary Figure 10), although ONO1301 did not activate cAMP signaling in Huh-7 cells (Supplementary Figure 11). A slight decrease of HCVcc egression, however, caused by the treatment with ONO1301 at high concentrations, might be of note. These results further supported our conclusion that TXAS-mediated signaling contributes to infectious HCV production, although the functional role of $PGI_2$ in this process still is unknown.

## Discussion

In this study, we showed that TXAS is involved in the development of infectious HCV. Administration of a TXAS inhibitor inhibited early stages of HCV proliferation postinfection in a chimeric mouse model. These results suggest that TXAS-mediated infectious HCV production is a potential target for novel anti-HCV therapies.

We first found that inhibiting COX1 and TXAS decreased the infectivity of HCVcc in the culture medium without any significant effects on viral genome replication and particle egression (Figures 2 and 3). In addition, we showed that inhibition of TXAS did not affect the release of infectious HCVcc from the cells (Figure 5). Thus, we concluded that TXAS probably regulates HCV particle maturation and the development of infectivity. Knockdown of apolipoprotein E, heat shock protein 70, and annexin A2 expression was shown previously to inhibit infectious HCVcc production.[26] Of note, decreased expression of these host factors reduced the production of HCVcc in the culture medium as well as intracellular HCVcc levels in HCVcc-producing cells, suggesting that TXAS is playing a different role in HCVcc production.

BASIC AND TRANSLATIONAL

Moreover, our results suggest that TXAS is a host factor that contributes only to the development of HCV infectivity.

A previous study reported that infectious HCVcc is produced near LDs.[11] The HCV proteins core and NS5A are located on and nearby LDs, respectively, suggesting a role in the production of infectious HCVcc.[11] Because LD localization of these proteins was not affected by the TXAS inhibitor (Figure 5*A*), TXAS probably is required after these viral proteins are recruited to LDs.

Several studies have shown that the buoyant density of infectious HCVcc differs slightly from that of noninfectious HCVcc.[11,27,28] Infectious and noninfectious HCVcc are found in lower- and higher-density fractions, respectively. In the present study, inhibition of TXAS reduced the amount of HCVcc in the lower-density fraction (fraction 6) containing the infectious particles, whereas levels of primarily noninfectious HCVcc particles in the higher-density fraction (fraction 5) were not affected (Figure 6). These results mirrored previously reported data about NS5A mutant HCVcc, which do not produce infectious particles.[11] These results suggest that TXAS might be required to produce infectious HCVcc near the LDs.

Studies with treatment with methyl-$\beta$-cyclodextrin or lipoprotein lipase have shown that changing the physicochemical properties of HCVcc,[28-30] in which the peak density fraction containing HCVcc shifted higher, diminished the infectivity of the particles.[29,30] Because TXAS inhibitors did not show the apparent shift to a higher density (Figure 6), future molecular analyses of HCVcc particles should be required to reveal the underlying structural mechanisms for HCV infectivity.

Prostanoids play various physiologic functions, including regulatory roles in muscle and blood vessels.[17] Although inhibition of TXAS decreased the infectivity of HCVcc (Figure 3), the identity of the relevant prostanoid and how that product functions in the development of infectious HCV are currently unclear. Because the treatment of $PGH_2$, a substrate of TXAS, caused the increase of infectious HCV production (Supplementary Figure 6), it seemed likely that the decrease of HCV infectivity is not due to an accumulation of $PGH_2$ caused by TXAS inhibition. Although we analyzed the total fatty acids in the HCV-infected Huh-7.5 cells treated with and without Ozagrel, the compositions of fatty acids, including arachidonic acid, were not largely different from each other (Supplementary Figure 12, the arachidonic acid is shown as C20:4$\omega$-6), suggesting that the effect of Ozagrel is not caused by major changes of fatty acid composition.

The activity of the TXAS product $TXA_2$ was not examined directly because its half-life is quite short.[31] Usually, $TXA_2$ activity is measured using stable agonists and antagonists of TP. We showed, however, that TP-mediated signaling is not related to the processes examined in the current study (Figure 4). It seemed likely that $TXA_2$ itself or an unidentified metabolite of $TXA_2$ mediates the development of HCV infectivity in a TP-independent manner. $PGI_2$ and the $PGD_2$ metabolite 15d-$PGJ_2$ have been identified as ligands of peroxisome proliferator activated receptor $\delta$ and $\gamma$, respectively.[32,33] Therefore, the TXAS product may act as a ligand of various nuclear receptors to regulate infectious HCV production. In primary human hepatocytes and liver of chimeric mice transplanted with human hepatocytes, the expression of human TP mRNA was not observed (Supplementary Figures 3*A* and 13), although it was detected in human liver tissue, consisting of many cell types (Supplementary Figure 13). It may be true, therefore, that the *TP* gene is not largely expressed in human hepatocytes in the liver as with Huh-7 cells. Taken together, it is probable that infectious HCV is produced in a TP-independent manner in human liver infected with HCV. Further studies regarding the TP-independent roles of TXAS products in hepatocytes may be required to elucidate the mechanisms of infectious HCV formation.

Recently, various drugs targeting viral proteins were developed, resulting in more HCV-specific therapeutic profiles than those of conventional drugs.[34] Monotherapy with an HCV-specific drug, however, sometimes fails to clear the HCV infection because of rapidly emerging resistant variants.[35] We found that a TXAS inhibitor and IP agonists suppressed early stage expansion of bbHCV postinfection of chimeric mice bearing human hepatocytes (Figure 7). These results clearly indicate that the TXAS inhibitor and IP agonist are novel candidates for anti-HCV drugs. In this experiment, the effects of an IP agonist and the TXAS inhibitor were compared because $TXA_2$ and IP agonists have opposite clinical effects.[20] This implies that the IP agonist may have suppressed the effects of TXAS in the bbHCV-infected transplanted human hepatocytes. Contrary to our expectations, however, neither siRNA-mediated knockdown of PGIS expression nor treatment with the IP agonist Beraprost affected HCV genome replication, particle egression, or HCVcc infectivity (Supplementary Figure 9). The responsiveness of Huh-7 cells to the IP agonist then was examined by monitoring activation of cAMP signaling, a pathway that normally is activated downstream of IP. The results show that Huh-7 cells were deficient in signaling from IP to intracellular cAMP production (Supplementary Figure 11). Although the therapeutic mechanism of action for the IP agonist in chimeric mice has not been clarified yet, the IP agonist may signal through IP to counteract $TXA_2$ signaling and suppress the effects of endogenous TXAS products on the formation of infectious HCV. In this in vivo experiment, the effect of drugs waned over time, especially in the case of Ozagrel. We examined the effect of Ozagrel on the secondary HCV propagation in the mice inoculated with the sera of the HCV infected mice treated with Ozagrel in the first drug treatment. The results showed that HCV proliferated in the secondarily infected chimeric mice irrespective of the treatment of Ozagrel (Supplementary Figure 14), suggesting that HCV proliferating in the chimeric mice with the first treatment

acquired the resistance against Ozagrel. We analyzed partial genomic sequences of the drug-resistant HCVs by the direct sequencing method. We found that 68 base substitutions, 10 of which were accompanied with amino acid substitution, were present in such HCV genomes, compared with those in the mice untreated with the drug (Supplementary Figure 15). This indicated that the HCV proliferating in the chimeric mouse treated with Ozagrel included a large number of base substitutions in the genome. Further study of such drug-resistant HCV, for example, the reverse genetic analysis using a recombinant HCV system, will help to reveal the molecular mechanisms of the medicinal effects of this drug and the infectious HCV production. Furthermore, these results show the need to find the optimum dose of TXAS inhibitor for effective therapy and to use this drug as one option with different action mechanisms for multidrug therapy.

## Supplementary Material

Note: To access the supplementary material accompanying this article, visit the online version of *Gastroenterology* at www.gastrojournal.org, and at http://dx.doi.org/10.1053/j.gastro.2013.05.014.

### References


1. Wasley A, Alter MJ. Epidemiology of hepatitis C: geographic differences and temporal trends. Semin Liver Dis 2000;20:1–16.
2. Younossi Z, Kallman J, Kincaid J. The effects of HCV infection and management on health-related quality of life. Hepatology 2007; 45:806–816.
3. Fried MW, Shiffman ML, Reddy KR, et al. Peginterferon alfa-2a plus ribavirin for chronic hepatitis C virus infection. N Engl J Med 2002; 347:975–982.
4. Gao M, Nettles RE, Belema M, et al. Chemical genetics strategy identifies an HCV NS5A inhibitor with a potent clinical effect. Nature 2010;465:96–100.
5. Chayama K, Takahashi S, Toyota J, et al. Dual therapy with the nonstructural protein 5A inhibitor, daclatasvir, and the nonstructural protein 3 protease inhibitor, asunaprevir, in hepatitis C virus genotype 1b-infected null responders. Hepatology 2012; 55:742–748.
6. Lin C, Kwong AD, Perni RB. Discovery and development of VX-950, a novel, covalent, and reversible inhibitor of hepatitis C virus NS3.4A serine protease. Infect Disord Drug Targets 2006;6:3–16.
7. Sarrazin C, Zeuzem S. Resistance to direct antiviral agents in patients with hepatitis C virus infection. Gastroenterology 2010; 138:447–462.
8. **Wakita T**, **Pietschmann T**, Kato T, et al. Production of infectious hepatitis C virus in tissue culture from a cloned viral genome. Nat Med 2005;11:791–796.
9. Lindenbach BD, Evans MJ, Syder AJ, et al. Complete replication of hepatitis C virus in cell culture. Science 2005;309:623–626.
10. **Zhong J**, **Gastaminza P**, Cheng G, et al. Robust hepatitis C virus infection in vitro. Proc Natl Acad Sci U S A 2005;102:9294–9299.
11. Miyanari Y, Atsuzawa K, Usuda N, et al. The lipid droplet is an important organelle for hepatitis C virus production. Nat Cell Biol 2007;9:1089–1097.
12. Aly HH, Watashi K, Hijikata M, et al. Serum-derived hepatitis C virus infectivity in interferon regulatory factor-7-suppressed human primary hepatocytes. J Hepatol 2007;46:26–36.
13. Aly HH, Qi Y, Atsuzawa K, et al. Strain-dependent viral dynamics and virus-cell interactions in a novel in vitro system supporting the life cycle of blood-borne hepatitis C virus. Hepatology 2009; 50:689–696.
14. Aly HH, Shimotohno K, Hijikata M. 3D cultured immortalized human hepatocytes useful to develop drugs for blood-borne HCV. Biochem Biophys Res Commun 2009;379:330–334.
15. Chockalingam K, Simeon RL, Rice CM, et al. A cell protection screen reveals potent inhibitors of multiple stages of the hepatitis C virus life cycle. Proc Natl Acad Sci U S A 2010;107:3764–3769.
16. Gastaminza P, Whitten-Bauer C, Chisari FV. Unbiased probing of the entire hepatitis C virus life cycle identifies clinical compounds that target multiple aspects of the infection. Proc Natl Acad Sci U S A 2010;107:291–296.
17. Bos CL, Richel DJ, Ritsema T, et al. Prostanoids and prostanoid receptors in signal transduction. Int J Biochem Cell Biol 2004; 36:1187–1205.
18. Little P, Skouteris GG, Ord MG, et al. Serum from partially hepatectomized rats induces primary hepatocytes to enter S phase: a role for prostaglandins? J Cell Sci 1988;91:549–553.
19. Rudnick DA, Perlmutter DH, Muglia LJ. Prostaglandins are required for CREB activation and cellular proliferation during liver regeneration. Proc Natl Acad Sci U S A 2001;98:8885–8890.
20. Waris G, Siddiqui A. Hepatitis C virus stimulates the expression of cyclooxygenase-2 via oxidative stress: role of prostaglandin E2 in RNA replication. J Virol 2005;79:9725–9734.
21. Tateno C, Yoshizane Y, Saito N, et al. Near completely humanized liver in mice shows human-type metabolic responses to drugs. Am J Pathol 2004;165:901–912.
22. Kushima Y, Wakita T, Hijikata M. A disulfide-bonded dimer of the core protein of hepatitis C virus is important for virus-like particle production. J Virol 2010;84:9118–9127.
23. Gastaminza P, Kapadia SB, Chisari FV. Differential biophysical properties of infectious intracellular and secreted hepatitis C virus particles. J Virol 2006;80:11074–11081.
24. Kamiya N, Iwao E, Hiraga N, et al. Practical evaluation of a mouse with chimeric human liver model for hepatitis C virus infection using an NS3-4A protease inhibitor. J Gen Virol 2010; 91:1668–1677.
25. Flavahan NA. Balancing prostanoid activity in the human vascular system. Trends Pharmacol Sci 2007;28:106–110.
26. Bartenschlager R, Penin F, Lohmann V, et al. Assembly of infectious hepatitis C virus particles. Trends Microbiol 2011;19:95–103.
27. Andre P, Komurian-Pradel F, Deforges S, et al. Characterization of low- and very-low-density hepatitis C virus RNA-containing particles. J Virol 2002;76:6919–6928.
28. Nielsen SU, Bassendine MF, Burt AD, et al. Association between hepatitis C virus and very-low-density lipoprotein (VLDL)/LDL analyzed in iodixanol density gradients. J Virol 2006; 80:2418–2428.
29. Aizaki H, Morikawa K, Fukasawa M, et al. Critical role of virion-associated cholesterol and sphingolipid in hepatitis C virus infection. J Virol 2008;82:5715–5724.
30. Shimizu Y, Hishiki T, Sugiyama K, et al. Lipoprotein lipase and hepatic triglyceride lipase reduce the infectivity of hepatitis C virus (HCV) through their catalytic activities on HCV-associated lipoproteins. Virology 2010;407:152–159.
31. Gryglewski RJ. Prostacyclin among prostanoids. Pharmacol Rep 2008;60:3–11.
32. Forman BM, Tontonoz P, Chen J, et al. 15-Deoxy-delta 12, 14-prostaglandin J2 is a ligand for the adipocyte determination factor PPAR gamma. Cell 1995;83:803–812.
33. Gupta RA, Tan J, Krause WF, et al. Prostacyclin-mediated activation of peroxisome proliferator-activated receptor delta in colorectal cancer. Proc Natl Acad Sci U S A 2000;97:13275–13280.
34. Pawlotsky JM, Chevaliez S, McHutchison JG. The hepatitis C virus life cycle as a target for new antiviral therapies. Gastroenterology 2007; 132:1979–1998.

35. Wohnsland A, Hofmann WP, Sarrazin C. Viral determinants of resistance to treatment in patients with hepatitis C. Clin Microbiol Rev 2007;20:23–38.

Author names in bold designate shared co-first authorship.

Received August 11, 2012. Accepted May 13, 2013.

*Reprint requests*

Address requests for reprints to: Makoto Hijikata, PhD, Laboratory of Human Tumor Viruses, Department of Viral Oncology, Institute for Virus Research, Kyoto University, 53, Kawaharacho, Shogoin, Sakyoku, Kyoto 606-8507, Japan. e-mail: mhijikat@virus.kyoto-u.ac.jp; fax: (81) 75-751-3998.

*Acknowledgments*

The authors thank Dr Michinori Kohara (Tokyo Metropolitan Institute of Medical Science, Tokyo, Japan) for providing anti-hepatitis C virus core antibody; Toyobo, Co (Osaka, Japan) for providing hollow fibers; Toray, Co (Tokyo, Japan) for providing Beraprost; and Dr Masayoshi Fukasawa (National Institute of Infectious Disease, Tokyo, Japan) for helpful discussion.

Present address of H.H.A.: Department of Virology 2, National Institute of Infectious Disease, Tokyo, Japan.

Transcript Profiling: The microarray data in this study was named "HuSE2, 2Dvs3D," and was registered in ArrayExpress. Accession number: E-MTAB-1491.

Nucleic acid sequences: Sequencing data in this study were named "BankIt1626925 Seq1" and "BankIt1626925 Seq3", and registered with GenBank. Accession numbers: KF006982 and KF006984, respectively.

*Conflicts of interest*

The authors disclose no conflicts.

*Funding*

Supported by grants-in-aid from the Ministry of Health, Labour and Welfare of Japan.

## Supplementary Materials and Methods

### *Preparation of Subcellular Fraction and Protein Detection With Western Blotting*

Subcellular fractions of HuS-E/2 cells and patient's tissues were prepared with the ProteoExtract Subcellular proteome Extraction Kit (Millipore, Billerica, MA) according to the manufacturer's protocol. Five micrograms of total protein of each fraction or whole-cell lysate of each cell was analyzed by Western blotting. Western blotting was performed as described previously.[1]

### *Collection of Total RNA and Cell Lysate From HCV-Infected Patients' Tissue*

Total RNA from patients' tissue was collected with RNeasy mini (Qiagen, Hilden, Germany). In brief, frozen tissues were homogenized in lysis buffer with a Power Masher (Nippi, Tokyo, Japan). Homogenized samples were used for RNA purification according to the manufacturer's protocol. Cell lysate from tissues were collected with RIPA buffer (Thermo Scientific, Waltham, MA) or the ProteoExtract Subcellular proteome Extraction Kit according to the manufacturer's protocol.

### *cAMP Reporter Assay*

Huh-7-derived and HuS-E/2 cells were transfected with pCRE-Luc (Agilent Technologies, Santa Clara, CA) using Fugene6 (Roche) and Effectene (Qiagen), respectively, essentially according to the manufacturers' protocols. Six hours and 2 days post-transfection of Huh-7-derived and HuS-E/2 cells, respectively, the culture medium was replaced with fresh medium containing one of the reagents. One and 3 day(s) post-transfection of Huh-7-derived and HuS-E/2 cells, respectively, luciferase activity in the cells was measured using a luciferase activity detection reagent (Promega, Madison, WI) and a Lumat LB 9507 luminometer (EG&G Berthold, Bad Wildbad, Germany).

### *Calcium Ion Quantification*

HEK293, Huh-7-derived, and HuS-E/2 cells were treated with the calcium ionosphere A23187 (Sigma-Aldrich) and the TP agonist U-46619 for 1 day. Calcium ion concentrations were quantified using a calcium assay kit (Cayman Chemical) according to the manufacturer's protocols.

### *Actin Polymerization Assay*

Activation of actin polymerization via TP was measured with fluorescein isothiocyanate-phalloidin (Sigma-Aldrich). After culture in lipid-free fresh medium, cells were stimulated with 10 $\mu$mol/L U46619 containing medium for 30, 60, and 180 seconds. Then, samples were stained with 10 $\mu$g/mL fluorescein isothiocyanate phalloidin, Fluorescent intensity at 520 nm was measured.

### *Fatty Acid Analysis*

Fatty acid analysis of HCV-infected Huh-7.5 cells treated with or without Ozagrel was performed by Toray Research Center, Inc, Tokyo, Japan using gas chromatography. Total fatty acid samples were extracted from the cells according to the Bligh-Dyer[2] method.

### *Secondary Infection Experiments in Chimeric Mice Transplanted Human Hepatocytes*

The chimeric mice were inoculated intravenously with patient serum including $1.0 \times 10^5$ genome titer of bbHCV (genotype 1b) as the first infection. Ozagrel was administered orally twice each day (300 $\mu$g/day) 1 week after the inoculation. The serum samples from those mice were collected at 5 weeks after starting the drug treatments, and used as inocula in the secondary infection experiment. Naive chimeric mice were inoculated with the collected chimeric mice serum including $1.0 \times 10^5$ genome titer of HCV. Administration of Ozagrel was started simultaneously. HCV-RNA levels in the blood of the chimeric mice at 1, 2, and 3 weeks after infection in secondary infection experiments were evaluated by qRT-PCR.

### *Determination of Nucleotide Sequence of HCV Genome After Treatment With Ozagrel*

Chimeric mice were inoculated secondarily with sera from HCV-infected chimeric mice with or without Ozagrel treatment. Sera of these chimeric mice treated with or without Ozagrel were collected 5 weeks after the inoculation and the start of the treatment. HCV genome sequences of these samples were determined by the direct sequencing method according to the protocol described previously.[3] HCV genomic sequences obtained from sera of mice with 2 different types of treatment were compared with each other. Mice with 2 different types of treatments were as follows: first, mice inoculated secondarily with sera from the first chimeric mouse without treatment were not treated with the drug (BankIt1626925 Seq3 in GenBank). Second, mice inoculated secondarily with sera from the first chimeric mouse with treatment were treated with the drug (BankIt1626925 Seq1 in GenBank). These sequencing data were registered with GenBank (http://www.ncbi.nlm.nih.gov/genbank/).

### Supplementary References

1. Kushima Y, Wakita T, Hijikata M. A disulfide-bonded dimer of the core protein of hepatitis C virus is important for virus-like particle production. J Virol 2010;84:9118-9127.
2. Bligh EG, Dyer WJ. A rapid method of total lipid extraction and purification. Can J Biochem Physiol 1959;37:911-917.
3. Kimura T, Imamura M, Hiraga N, et al. Establishment of an infectious genotype 1b hepatitis C virus clone in human hepatocyte chimeric mice. J Gen Virol 2008;89:2108-2113.

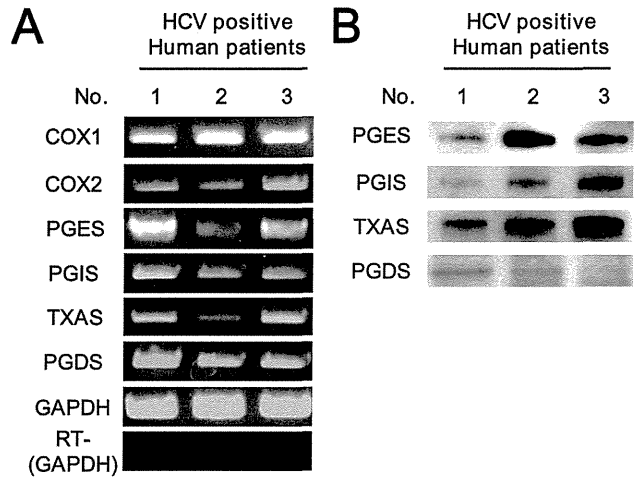


**Supplementary Figure 1.** Protein and mRNA levels of PG synthases in HCV-infected patient tissue. (*A* and *B*) mRNA expression and protein levels of PG synthases in HCV-infected patient tissue. Representative results from 2 independent experiments are shown.

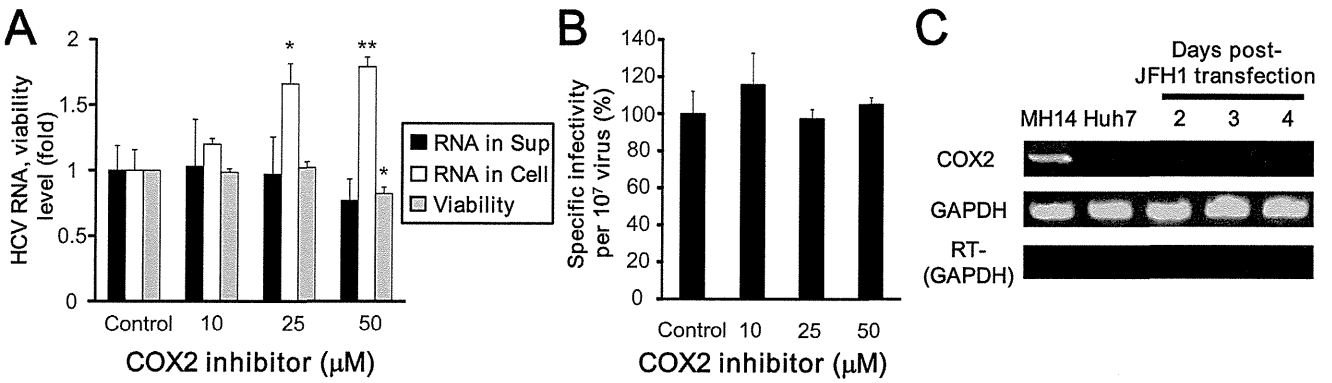


**Supplementary Figure 2.** Effects of COX2 inhibitor 1 on infectious HCV production. (*A*) Effects of COX2 inhibitor 1 on HCV-RNA levels in the HCVcc-producing cell-culture system. Levels of HCV RNA in medium (*black bars*) and cells (*white bars*) treated with or without COX2 inhibitor 1 were assessed with qRT-PCRs and plotted as amounts relative to results observed with control cells (control). Mean cell viability ± SD for each sample condition also is plotted (*gray bars*). (*B*) Effects of COX2 inhibitor 1 on the infectivity of HCVcc produced using the cell-culture system. (*C*) Expression of COX2 mRNA in MH14 (positive control), Huh-7, and JFH1-transfected Huh-7 cells. *Differs from control, $P < .01$; **differs from control, $P < .001$.

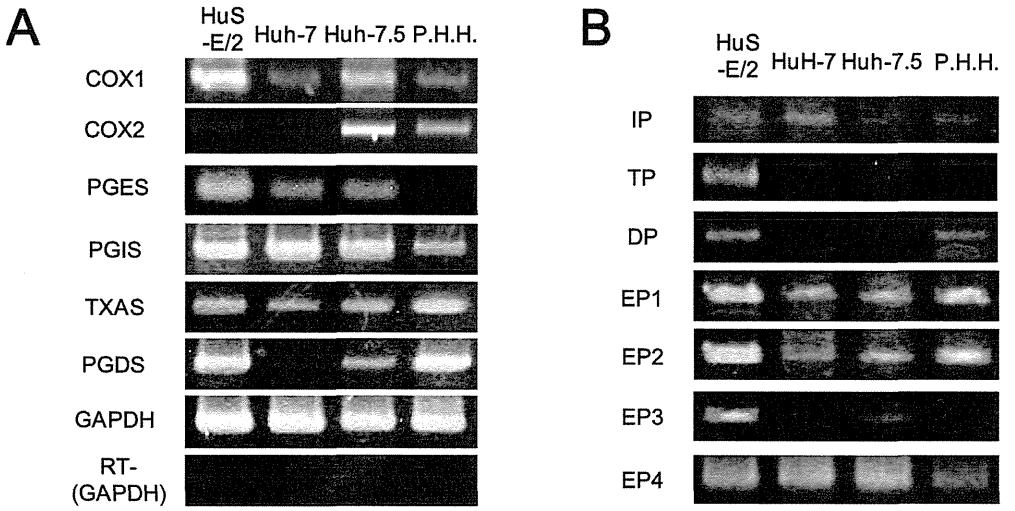


**Supplementary Figure 3.** Expression of PG synthase and PG-receptor mRNA in immortalized and primary hepatocyte cell lines. (*A* and *B*) mRNA expression levels of various PG synthases and PG receptors in HuS-E/2 cells, Huh-7 cells, Huh-7.5 cells, and primary human hepatocytes were analyzed in RT-PCRs. Representative results from 2 independent experiments are shown.

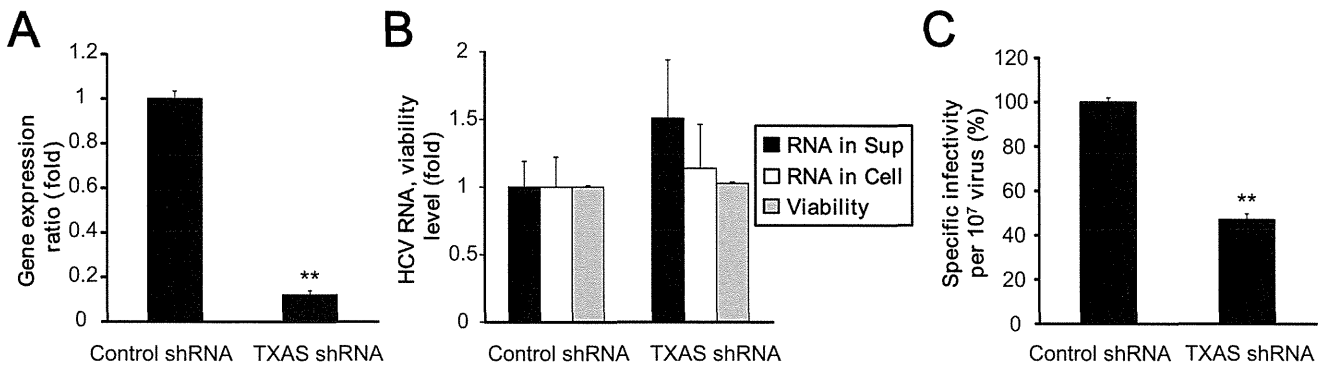


**Supplementary Figure 4.** Effects of short hairpin RNA (shRNA)-mediated knockdown of TXAS mRNA levels on infectious HCV production. (*A*) Knockdown of TXAS mRNA levels using shRNA. (*B*) Effects of TXAS-specific shRNA on HCV-RNA levels in the HCVcc-producing cell culture system. Levels of HCV RNA in medium (*black bars*) and cells (*white bars*) treated with control or TXAS-specific shRNA were assessed with qRT-PCRs and plotted as amounts relative to results observed with control shRNA–treated cells (control). Mean cell viability ± SD for each sample condition also is plotted (*gray bars*). (*C*) Effects of TXAS-specific shRNA on the infectivity of HCVcc produced using the cell-culture system. **Differs from control, $P < .001$.

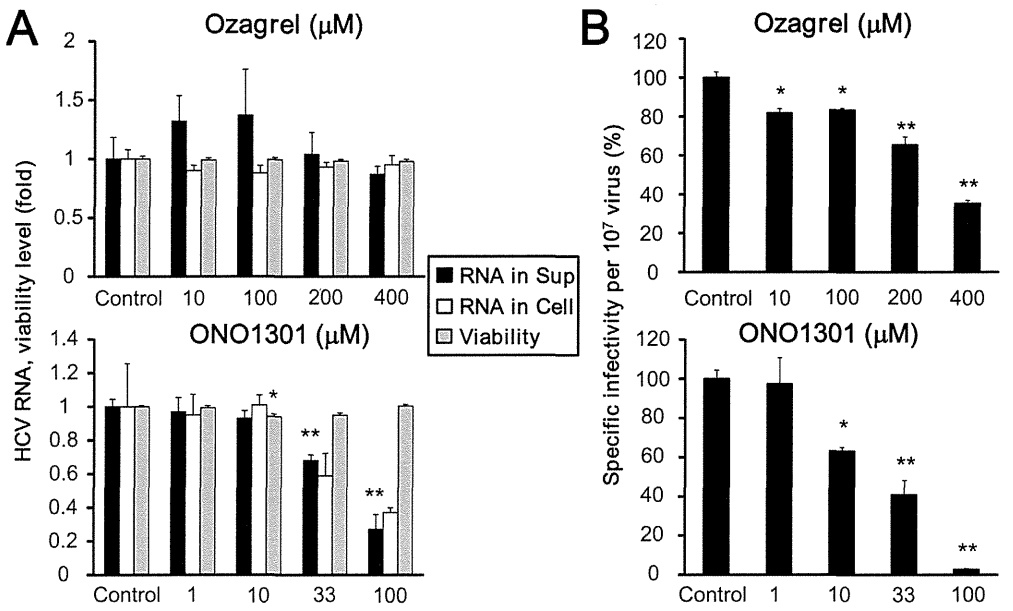


**Supplementary Figure 5.** Effects of Ozagrel and ONO1301 on the infectivity of HCVcc produced from J6/JFH1-transfected Huh-7.5 cells. (*A*) Effects of Ozagrel (*upper panel*) and ONO1301 (*lower panel*) on HCV-RNA levels in HCVcc-producing cell cultures. Levels of HCV RNA in the medium (*black bars*) and cells (*white bars*) treated with Ozagrel or ONO1301 cells were assessed in qRT-PCRs and plotted as the amount relative to results from untreated cells (control). Mean cell viability ± SD for each sample condition also is plotted (*gray bars*). (*B*) Effects of Ozagrel (*upper panel*) and ONO1301 (*lower panel*) on the infectivity of HCVcc produced in the cell-culture system. *Differs from control, $P < .01$; **differs from control, $P < .001$.

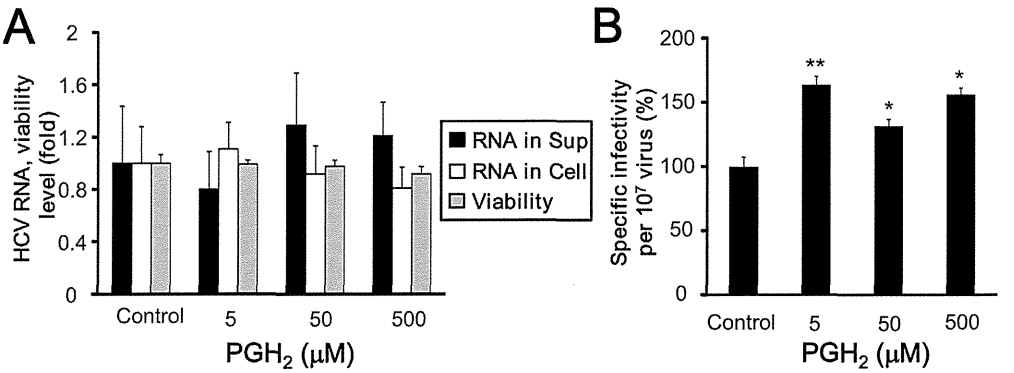


**Supplementary Figure 6.** Effects of $PGH_2$ on infectious HCV production. (*A*) Effects of $PGH_2$ on HCV-RNA levels in the HCVcc-producing cell-culture system. Levels of HCV RNA in medium (*black bars*) and cells (*white bars*) treated with or without $PGH_2$ were assessed with qRT-PCRs and plotted as amounts relative to results observed with control cells (control). Mean cell viability ± SD for each sample condition also is plotted (*gray bars*). (*B*) Effects of $PGH_2$ on the infectivity of HCVcc produced using the cell culture system. *Differs from control, $P < .01$; **differs from control, $P < .001$.

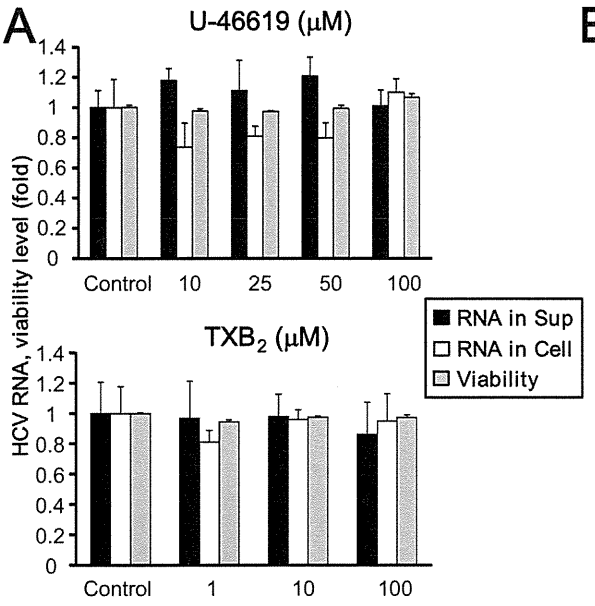


**Supplementary Figure 7.** Effects of U-46619 and $TXB_2$ on infectious HCV production. (*A*) Effects of U-46619 (*upper panel*) and $TXB_2$ (*lower panel*) on HCV-RNA levels in HCVcc-producing cell cultures. Levels of HCV RNA in the medium (*black bars*) and cells (*white bars*) treated with U-46619 or $TXB_2$ were assessed in qRT-PCRs and plotted as the amount relative to results observed with untreated cells (control). Mean cell viability ± SD for each sample condition also is plotted (*gray bars*). (*B*) Effects of U-46619 (*upper panel*) and $TXB_2$ (lower panel) on the infectivity of HCVcc produced in the cell-culture system were assessed.

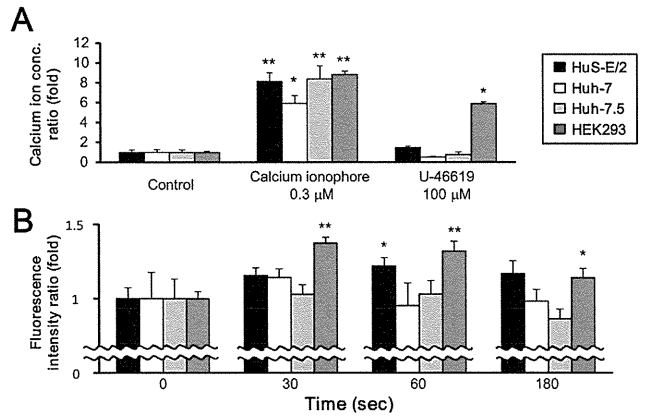


**Supplementary Figure 8.** Effects of U-46619 on HuS-E/2, Huh-7, Huh-7.5, and HEK293 cell lines via TP. (*A*) Concentrations of intracellular calcium ions were measured in HuS-E/2 (*black bars*), Huh-7 (*white bars*), Huh-7.5 (*gray bars*), and HEK293 (*dark gray bars*) cells treated with or without a calcium ionophore or U-46619. Calcium ion concentrations relative to those in mock-treated cells (control) were determined from triplicate wells in 2 independent experiments and are shown as means ± SD. (*B*) Actin polymerization after U-46619 treatment was measured with fluorescein isothiocyanate (FITC)-labeled phalloidin. *Differs from control, $P < .01$; **differs from control, $P < .001$.

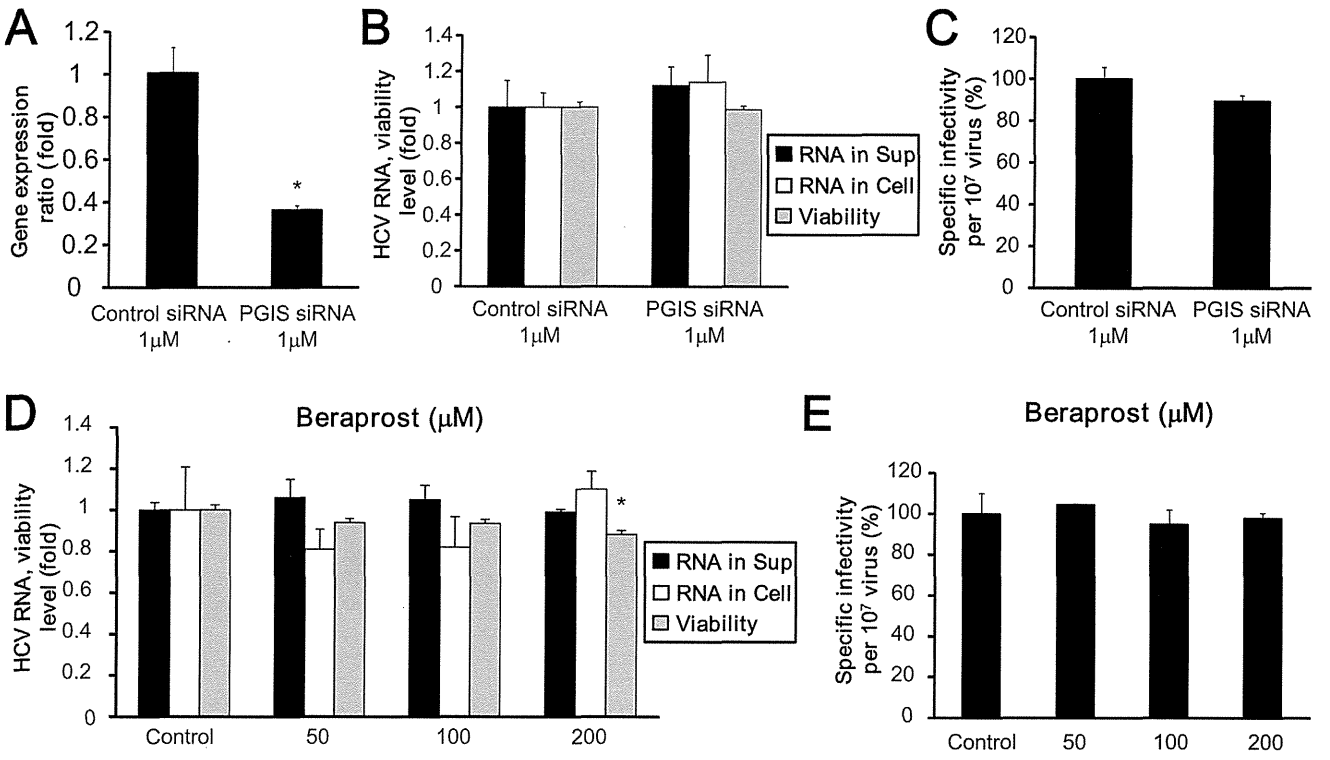


**Supplementary Figure 9.** Effects of $PGI_2$ on infectious HCV production. (*A*) siRNA-mediated knockdown of PGIS expression. (*B*) Effects of PGIS-specific siRNA on HCV-RNA levels in HCVcc-producing cell cultures. Levels of HCV RNA in medium (*black bars*) and cells (*white bars*) treated with control or PGIS-specific siRNA were assessed in qRT-PCR and are plotted as amounts relative to results obtained with control siRNA–treated cells (control). Mean cell viability ± SD for each sample condition also is plotted (*gray bars*). (*C*) Effects of PGIS-specific siRNA on the infectivity of HCVcc produced in the cell-culture system. (*D*) Effects of Beraprost on HCV-RNA levels in HCVcc-producing cell cultures. Levels of HCV RNA in medium (*black bars*) and HCVcc-producing Huh-7 cells (*white bars*) treated with Beraprost were assessed in qRT-PCRs and plotted as amounts relative to results obtained with untreated cells (control). Mean cell viability ± SD for each sample condition also is plotted (*gray bars*). (*E*) Effects of Beraprost on the infectivity of HCVcc in culture medium from HCVcc-producing cell cultures were assessed. *Differs from control, $P < .01$.

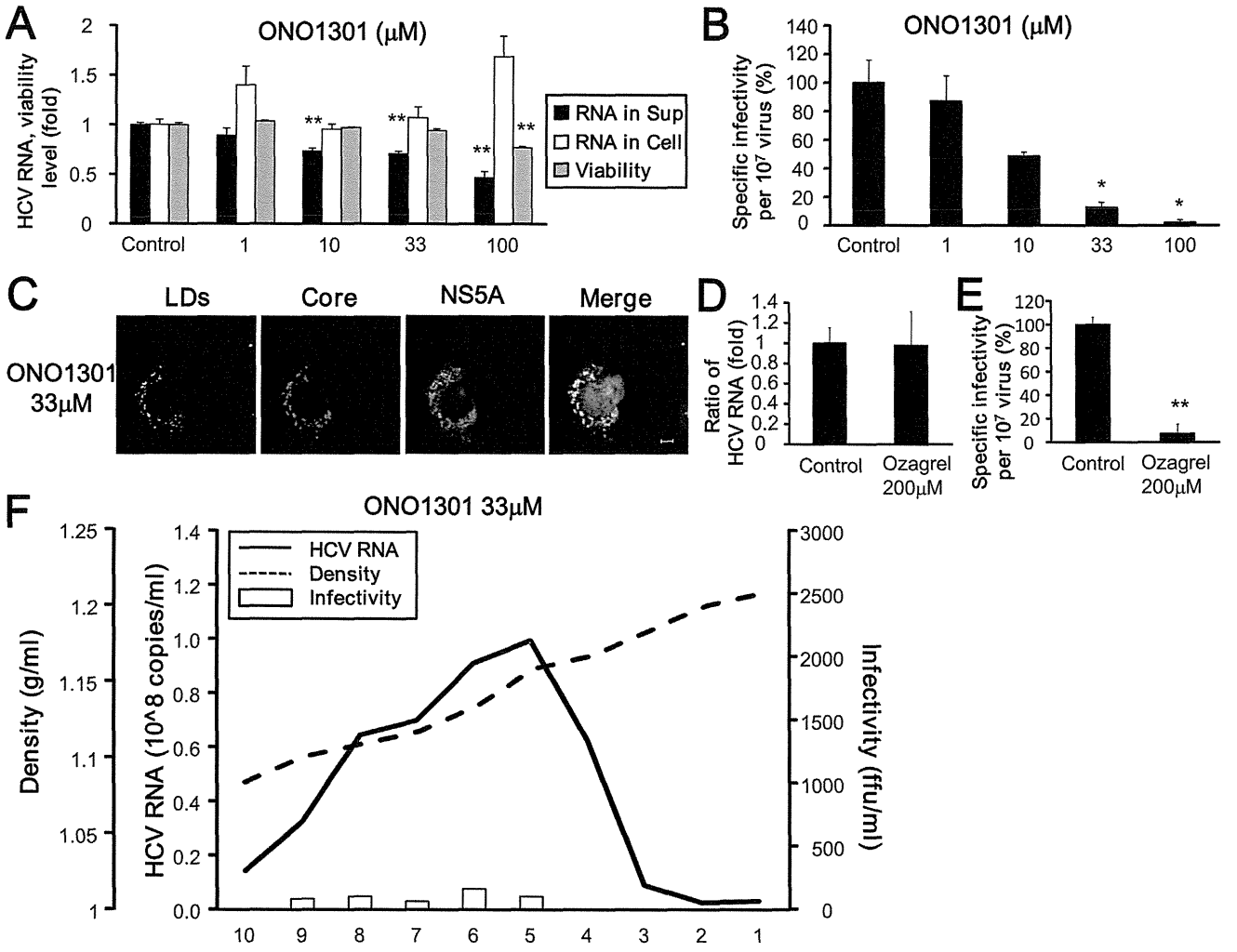


**Supplementary Figure 10.** Effects of ONO1301 on HCV lifecycle. (*A*) Levels of HCV RNA in medium (*black bars*) and cells (*white bars*) treated with or without ONO1301 were assessed. Mean cell viability ± SD for each sample condition also is plotted (*gray bars*). (*B*) The infectivity of HCVcc in culture medium from HCVcc-producing cell cultures treated with or without ONO1301 was assessed. (*C*) Subcellular locations of HCV core and NS5A proteins around LDs in the presence of ONO1301. Scale bars, 5 μm. (*D* and *E*) Levels and infectivity of intracellular HCV obtained from the cells treated with ONO1301. (*F*) Buoyant density of HCVcc obtained using cells treated with ONO1301. HCV RNA (*solid line*), fraction density (*dotted line*), and HCV infectivity (*white bars*) in each fraction collected by ultracentrifugation. *Differs from control, $P < .01$; **differs from control, $P < .001$.

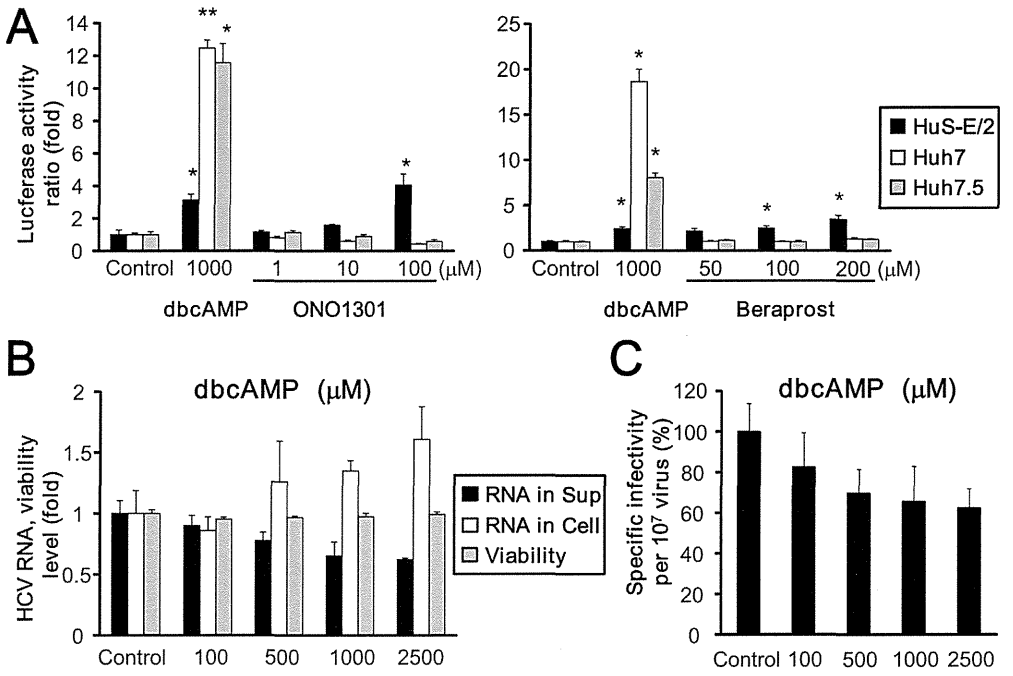


**Supplementary Figure 11.** Effects of dibutyryl cAMP (dbcAMP) on cell cultures producing JFH1 HCVcc. (*A*) HuS-E/2 (*black bars*), Huh-7 (*white bars*), and Huh-7.5 (*gray bars*) cells were transfected with CRE-Luc plasmid. Then, the luciferase activity in each sample was measured. Values were obtained from quadruplicate wells in 2 independent experiments and are shown as means ± SD. (*B*) Effects of dbcAMP on HCV-RNA levels in HCVcc-producing cell cultures. Levels of HCV RNA in medium (*black bars*) and cells treated with dbcAMP (*white bars*) were assessed in qRT-PCRs and plotted as amounts relative to results obtained with mock-treated cells (control). Mean cell viability ± SD for each sample condition also is plotted (*gray bars*). (*C*) Effects of dbcAMP on the infectivity of HCVcc produced using the cell-culture system. *Differs from control, $P < .01$; **differs from control, $P < .001$.

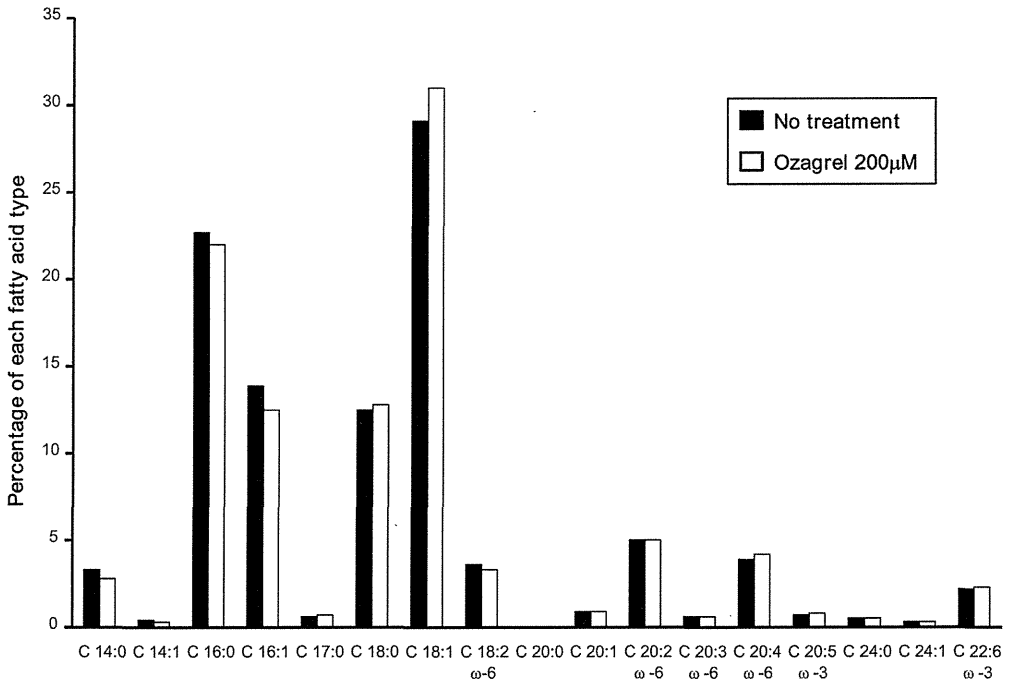


**Supplementary Figure 12.** Comparison of composition of fatty acids in HCV-infected Huh-7.5 cells with or without Ozagrel treatment.

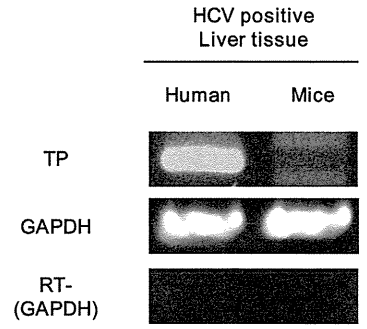


**Supplementary Figure 13.** Expression of TP mRNA in liver tissues from human patients and chimeric mice infected with HCV.

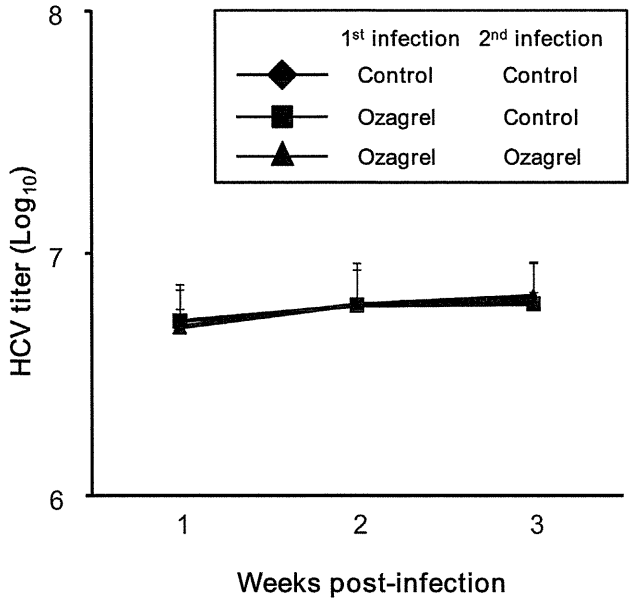


**Supplementary Figure 14.** Secondary infection of HCV derived from the chimeric mice model. Data are presented as means ± SD for 4 samples.

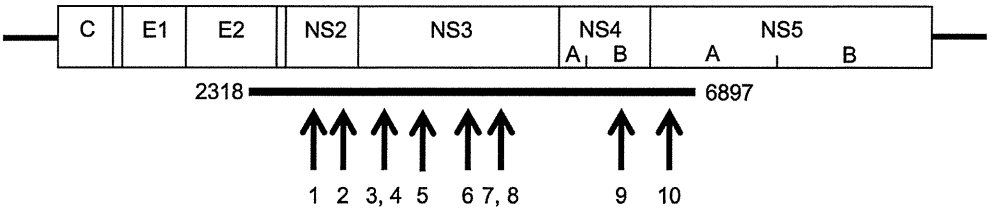


**Supplementary Figure 15.** Base substitutions in HCV genome collected from mice serum during a secondary infection. HCV genomic sequences from mice sera with Ozagrel treatment during primary and secondary infection was compared with those from mice without any treatment during both infection experiments. The region of obtained HCV genomic sequences is indicated (*thick bar*). The nucleotide positions of each base substitution are shown (*arrows*). Positions of base substitutions, and types of base substitution and amino acid replacement are listed in the *lower panel*.

| Number of substitution point | Position of nucleotide | Single base substitution | Amino acid replacement |
|---|---|---|---|
| 1 | 3192 | A→G | Asparagine→Aspartic acid |
| 2 | 3264 | A→G | Isoleucine→Valine |
| 3<br>4 | 3596<br>3597 | T→A<br>C→T | Phenylalanine→Tyrosine |
| 5 | 3859 | C→T | Serine→Leucine |
| 6 | 4283 | G→A | Methionine→Isoleucine |
| 7<br>8 | 4437<br>4439 | G→A<br>T→C | Glycine→Serine |
| 9 | 5886 | G→A | Valine→Methionine |
| 10 | 6747 | G→A | Alanine→Threonine |

**Supplementary Table 1.** Primer Sequences and Parameters in RT-PCR Experiments

| Genes | Primer Sequence 5′-3′ | Product size (bp) | Annealing Temperture | Cycle |
|---|---|---|---|---|
| COX1 | F: GCAGCTGAGTGGCTATTTCC<br>R: ATCTCCCGAGACTCCCTGAT | 324 | 60 | 32 |
| COX2 | F: GCAGTTGTTCCAGACAAGCA<br>R: GGTCAATGGAAGCCTGTGAT | 383 | 60 | 35 |
| PGES | F: GAAGAAGGCCTTTGCCAAC<br>R: GGAAGACCAGGAAGTGCATC | 200 | 62 | 35 |
| PGDS | F: AAGGCGGCGTTGTCCATGTGCAAGTC<br>R: ATTGTTCCGTCATGCACTTATC | 400 | 55 | 40 |
| PGIS | F: TCCTGGACCCACACTCCTAC<br>R: GCGAAAGGTGTGGAAGACAT | 395 | 60 | 40 |
| TXAS | F: TCTGCATCCCCAGACCTATC<br>R: ATAGCCAGCGATGAGGAAGA | 374 | 60 | 40 |
| GAPDH | F: ATGGGGAAGGTGAAGGTCGG<br>R: TGGAGGGATCTCGCTCCTGG | 250 | 60 | 40 |
| EP1 | F: GGTATCATGGTGGTGTCGTG<br>R: GGCCTCTGGTTGTGCTTAGA | 324 | 60 | 40 |
| EP2 | F: AGGAGAGGGGAAAGGGTGT<br>R: TCTTAATGAAATCCGACAACAGAG | 267 | 60 | 40 |
| EP3 | F: GACAGTCACCTTTTCCTGCAAC<br>R: AGGCGAACAGCTATTAAGAAGAAG | 276 | 60 | 40 |
| EP4 | F: CAGGACATCTGAGGGCTGAC<br>R: GTAGAAGGTCGTCTCCTTCTGCTC | 269 | 60 | 40 |
| DP | F: GCAACCTCTATGCGATGCAC<br>R: GGGTCCACAATTGAAATCAC | 292 | 60 | 32 |
| IP | F: AAGACTGGAGAGCCCAGACC<br>R: CCACGAACATCAGGGTGCTG | 161 | 60 | 40 |
| TP | F: CAGATGAGGTCTCTGAAGGTGTG<br>R: CAGAGGAAGGTGAGGAAGGAG | 304 | 60 | 40 |

NOTE. RT-PCRs were performed as follows: 25–40 cycles of 95°C for 30 seconds, 55–62°C for 30 seconds, and 72°C for 1 minute.

**Supplementary Table 2.** Primer Sequences and Parameters in qRT-PCR Experiments

| Genes | Primer Sequence 5′-3′ | Product Size (bp) |
|---|---|---|
| COX1 | F: TCCGGTTCTTGCTGTTCCTG<br>R: TCACACTGGTAGCGGTCAAG | 151 |
| PGES | F: CATCCTCTCCCTGGAAATCTCG<br>R: CCGCTTCCTACTGTGACCC | 129 |
| PGDS | F: CCTGTCCACCTTGCACAGTC<br>R: TCATGCTTCGGTTCAGGACG | 123 |
| PGIS | F: GCAGTGTCAAAAGTCGCCTG<br>R: ACTCTCCAGCCATTTGCTCC | 83 |
| TXAS | F: TTTGCTTGGTTGCCTGTTCC<br>R: CCAGAGTGGTGGTCTTCCAG | 99 |
| GAPDH | F: GACAGTCAGCCGCATCTTCT<br>R: GCGCCCAATACGACCAAATC | 104 |

NOTE. qRT-PCRs were performed as follows: 40 cycles of 95°C for 5 seconds, 60°C for 34 seconds.

Journal of Virology

# Hepatitis C Virus Infection Induces Inflammatory Cytokines and Chemokines Mediated by the Cross Talk between Hepatocytes and Stellate Cells

**Hironori Nishitsuji, Kenji Funami, Yuko Shimizu, Saneyuki Ujino, Kazuo Sugiyama, Tsukasa Seya, Hiroshi Takaku and Kunitada Shimotohno**

***J. Virol.* 2013, 87(14):8169. DOI: 10.1128/JVI.00974-13.**
**Published Ahead of Print 15 May 2013.**

JVI
Journals.ASM.org

# Hepatitis C Virus Infection Induces Inflammatory Cytokines and Chemokines Mediated by the Cross Talk between Hepatocytes and Stellate Cells

Hironori Nishitsuji,[a] Kenji Funami,[b] Yuko Shimizu,[a] Saneyuki Ujino,[a] Kazuo Sugiyama,[c] Tsukasa Seya,[b] Hiroshi Takaku,[d] Kunitada Shimotohno[a]

Research Center for Hepatitis and Immunology, National Center for Global Health and Medicine, Ichikawa, Chiba, Japan[a]; Department of Microbiology and Immunology, Hokkaido University Graduate School of Medicine, Kita, Sapporo, Japan[b]; Center for Integrated Medical Research, Keio University, Shinjuku-ku, Tokyo, Japan[c]; Department of Life and Environmental Sciences, Chiba Institute of Technology, Narashino-shi, Chiba, Japan[d]

**Inflammatory cytokines and chemokines play important roles in inflammation during viral infection. Hepatitis C virus (HCV) is a hepatotropic RNA virus that is closely associated with chronic liver inflammation, fibrosis, and hepatocellular carcinoma. During the progression of HCV-related diseases, hepatic stellate cells (HSCs) contribute to the inflammatory response triggered by HCV infection. However, the underlying molecular mechanisms that mediate HSC-induced chronic inflammation during HCV infection are not fully understood. By coculturing HSCs with HCV-infected hepatocytes *in vitro*, we found that HSCs stimulated HCV-infected hepatocytes, leading to the expression of proinflammatory cytokines and chemokines such as interleukin-6 (IL-6), IL-8, macrophage inflammatory protein 1α (MIP-1α), and MIP-1β. Moreover, we found that this effect was mediated by IL-1α, which was secreted by HSCs. HCV infection enhanced production of CCAAT/enhancer binding protein (C/EBP) β mRNA, and HSC-dependent IL-1α production contributed to the stimulation of C/EBPβ target cytokines and chemokines in HCV-infected hepatocytes. Consistent with this result, knockdown of mRNA for C/EBPβ in HCV-infected hepatocytes resulted in decreased production of cytokines and chemokines after the addition of HSC conditioned medium. Induction of cytokines and chemokines in hepatocytes by the HSC conditioned medium required a yet to be identified postentry event during productive HCV infection. The cross talk between HSCs and HCV-infected hepatocytes is a key feature of inflammation-mediated, HCV-related diseases.**

Hepatitis C virus (HCV) can cause chronic liver disease, which can progress to fibrosis, cirrhosis, and hepatocellular carcinoma (HCC) (1). Clearance of HCV during the acute phase of infection is associated with a robust CD4 and CD8 T-cell response to multiple viral epitopes (2). However, clearance of HCV infection often fails because of an intermediate cytotoxic T-cell response that is unable to eliminate the infection but causes hepatocyte destruction. T-cell-mediated hepatocytotoxicity poses a high risk for progression to chronic liver inflammation and damage (3). During chronic HCV infection, chemokine-chemokine receptor interactions are particularly important for the recruitment of T cells to sites of inflammation in the liver. Liver-infiltrating lymphocytes in HCV patients exhibit increased expression of CXCR3 and CCR5 (4). Moreover, intrahepatic chemokines, such as RANTES, macrophage inflammatory protein 1α (MIP-1α), MIP-1β, and IP-10, are elevated in HCV patients (5), and intrahepatic proinflammatory cytokine levels are correlated with the severity of inflammation and liver fibrosis (6).

The induction of proinflammatory cytokines and chemokines is triggered by viral proteins and double-stranded RNA (dsRNA) from HCV. The HCV core protein induces inflammatory cytokines through the STAT3 signaling pathway (7). Retinoic acid-inducible gene I (RIG-I) and Toll-like receptor 3 (TLR-3) are cellular sensors that recognize HCV dsRNA, resulting in production of chemokines such as interleukin-8 (IL-8), RANTES, MIP-1α, and MIP-1β (8, 9). Recently, an alternative mechanism for HCV-induced inflammation was reported. It was demonstrated that NS5B, the viral RNA-dependent RNA polymerase (RdRp), catalyzes production of small RNA species that trigger an innate immune response, leading to the production of both interferon (IFN) and inflammatory cytokines (10).

Hepatic stellate cells (HSCs) represent 5 to 8% of the total human liver cells and reside in the Disse space (11). Activation or transdifferentiation of HSCs is regulated by growth factors, including transforming growth factor β (TGF-β), which are associated with pathological conditions such as liver injury, cirrhosis, and cancer (11, 12). During liver injury, quiescent HSCs become activated and convert into highly proliferative, myofibroblast-like cells, which produce inflammatory and fibrogenic mediators (13). In a human hepatoma model, the cross talk between tumor hepatocytes and activated HSCs induced an inflammatory response, and the amounts of cytokines and chemokines associated with hepatocyte-HSC cross talk correlated to HCC progression (14).

Although direct induction of liver inflammation by HCV infection through cellular sensors or HCV proteins is well documented, little is known about the mechanisms governing the proinflammatory cytokines and chemokines that are produced during the interactions between HCV-infected hepatocytes and HSCs. Here, we show that HSCs can act as an inflammatory mediator to HCV-infected cells. Infection of hepatocytes with HCV

Received 9 April 2013 Accepted 9 May 2013
Published ahead of print 15 May 2013
Address correspondence to Hironori Nishitsuji, lbnishitsuji@hospk.ncgm.go.jp, or Kunitada Shimotohno, lbshimotohno@hospk.ncgm.go.jp.

doi:10.1128/JVI.00974-13

resulted in increased CCAAT/enhancer binding protein (C/EBPβ) production. Conditioned medium (CM) from HSCs induced hepatocyte production of inflammatory cytokines and chemokines, such as IL-6, IL-8, and MIP-1β, which are potential targets of C/EBPβ. Stimulation of these cytokines and chemokines in HCV-infected cells by HSC CM was suppressed by knockdown of mRNA for C/EBPβ. From the chemokines secreted by HSCs, IL-1α was identified as the inducer of MIP-1β. These results suggest HSCs may contribute to virus infection-associated liver inflammation through cross talk with HCV-infected hepatocytes.

## MATERIALS AND METHODS

**Cells.** LX2 cells (kindly provided by S. Friedman), NP-2-CCR5 cells (kindly provided by T. Hoshino), and Huh7.5 cells (kindly provided by C. Rice) were cultured in Dulbecco's modified Eagle's medium (DMEM) (Invitrogen) supplemented with 10% fetal bovine serum (FBS), 100 μg/ml penicillin and streptomycin, and 100 U/ml nonessential amino acids (Invitrogen). To maintain the quality of the cells, stored frozen stocks were thawed every 3 months and used in the experiments.

**Plasmids.** DNA fragments encoding each of the HCV nonstructural proteins were generated from a full-length cDNA clone of JFH1 by PCR. The fragments were cloned into pCAG-GS/N-Flag, in which the sequence encoding a Flag tag is inserted at the 5′ terminus of the cloning site of pCAG-GS.

**Virus.** Infectious HCV in cell culture (HCVcc) was produced by transfection of Huh7.5 cells with *in vitro*-transcribed RNA derived from JFH1 (kindly provided by T. Wakita) or TNS2J1 (the chimeric HCV genome containing HCV-1b in the structure region and JFH1 non-structural-protein-coding regions). UV-irradiated JFH1 was prepared by irradiation with a UV lamp of 254-nm wavelength at a distance of 6 cm for 1 min.

**HCV infection.** Huh7.5 cells were infected with JFH1 at a multiplicity of infection (MOI) of 5. Under this condition, 80 to 90% of the cells became positive for HCV core protein after 3 days.

**Preparation of conditioned medium from Huh7.5 or LX2 cells.** Huh7.5 or LX2 cells ($1 \times 10^6$) were seeded in 10 ml of medium in a 100-mm dish for 3 days. Supernatants were collected and filtered through 0.45-μm-pore-size filters.

**Chemotaxis of NP-2-CCR5 cells.** A 60-fold concentration of Huh7.5 or LX2 CM was generated by tapping in a filter membrane that cut off the 100-kDa-molecular-mass marker protein (100,000-molecular-weight-cutoff filter) and was used for experimental stimulations. Huh7.5 or JFH1-infected Huh7.5 cells (Huh7.5/JFH1 cells) were treated with each concentrated CM. After 24 h of treatment, the medium was changed to serum-free DMEM for 24 h and then used for chemotaxis assays. Chemotaxis of NP-2-CCR5 cells was measured in a 48-well chemotaxis chamber (Neuro Probe). The chamber consisted of a 48-well upper chamber and a 48-well lower chamber separated by a polycarbonate filter (pore size, 8 μm) coated with rat tail collagen. The lower wells were filled with each conditioned medium. The NP-2-CCR5 cells were washed and suspended in serum-free DMEM in the absence or presence of 0.1 nM maraviroc and then divided in the upper wells (5,000 cells per well). After incubation at 37°C for 180 min, the cells that had migrated into the lower well of the 48-well chemotaxis chamber were counted by Diff-Quik staining.

**Quantitative RT-PCR.** Total RNA was extracted from cells using RNeasy minikits (Qiagen), and cDNA was prepared with SuperscriptIII (Invitrogen) using oligo(dT) primers. Quantitative real-time PCR (qRT-PCR) was performed with Fast SYBR green master mix (Applied Biosystems), and fluorescent signals were analyzed with the Fast RT-PCR system (Applied Biosystems). The PCR primer pairs are described in Table 1.

**siRNA transfection.** Small interfering RNA (siRNA) was transfected using Lipofectamine RNAiMAX reagent (Invitrogen) according to the manufacturer's protocol. The duplex nucleotides of siRNA specific to the mRNA for C/EBPβ (5′-GAAGAAACGUCUAUGUGUA-3′) and the Mission siRNA universal negative control were purchased from Sigma. Synthetic siRNA specific to mRNA for IL-1 receptor-associated kinase 1 (IRAK1) (5′-CCCGGGCAAUUCAGUUUCUACAUCA-3′) and the Stealth RNA interference (RNAi) negative control duplex were purchased from Invitrogen.

TABLE 1 Real-time PCR primers

| Primer | Sequence (5′–3′) |
|---|---|
| CXCL1-F | GCAGGGAATTCACCCCAAGAAC |
| CXCL1-R | CTATGGGGGATGCAGGATTGAG |
| CXCL2-F | CCAACTGACCAGAAGGAAGGAG |
| CXCL2-R | ATGGCCTCCAGGTCATCATCAG |
| CXCL5-F | TGAGAGAGCTGCGTTGCGTTTG |
| CXCL5-R | TTCCTTCCCGTTCTTCAGGGAG |
| CXCL6-F | CTGCGTTGCACTTGTTTACGCG |
| CXCL6-R | GGGTCCAGACAAACTTGCTTCC |
| IL-1alpha-F | AGCTATGGCCCACTCCATGAAG |
| IL-1alpha-R | ACATTAGGCGCAATCCAGGTGG |
| IL-6-F | CCCCCAGGAGAAGATTCCAAAG |
| IL-6-R | TTCTGCCAGTGCCTCTTTGCTG |
| IL-7-F | ATTCCGTGCTGCTCGCAAGTTG |
| IL-7-R | AACCTGGCCAGTGCAGTTCAAC |
| IL-8-F | CTGTTAAATCTGGCAACCCTAGTCT |
| IL-8-R | CAAGGCACAGTGGAACAAGGA |
| MIP-1alpha-F | GCTGACTACTTTGAGACGAGC |
| MIP-1alpha-R | CCAGTCCATAGAAGAGGTAGC |
| MIP-1beta-F | CAGCGCTCTCAGCACCAATGG |
| MIP-1beta-R | GATCAGCACAGACTTGCTTGCTTC |
| C/EBP-beta-F | CTCGCAGGTCAAGAGCAAG |
| C/EBP-beta-R | GACAGCTGCTCCACCTTCTT |
| Collagen-F | AACATGACCAAAAACCAAAAGTG |
| Collagen-R | CATTGTTTCCTGTGTCTTCTGG |
| IL-1R-F | CCTGTCTTATGGCGTTGCAGGC |
| IL-1R-R | AGTGCCCTGGGCTGCTATTGAC |

**Cytokine antibody array.** LX2 cells ($1 \times 10^6$) were seeded in 10 ml of medium in a 100-mm dish for 2 days. The supernatant was then changed to 0.2% FBS-DMEM. Two days after incubation, the supernatants were collected and then concentrated by using a 100,000-molecular-weight-cutoff filter. The trapped and flowthrough fractions were dialyzed with phosphate-buffered saline (PBS) for 18 h. The amount of protein in each fraction was determined using a bicinchoninate protein assay kit (Nacalai Tesque). Three milligrams of each fraction was subjected to the cytokine antibody array.

The expression levels of 507 human proteins in the trap and flowthrough fractions from the LX2 cells were determined using biotin label-based human antibody array I (Raybiotech) according to the manufacturer's protocol.

## RESULTS

**LX2 cells induce MIP-1β expression in JFH1-infected Huh7.5 cells.** Our preliminary results indicated that coculturing human hepatic stellate cells (HSCs) with HCV-infected cells stimulated the expression of MIP-1β, which was found to be one of most upregulated chemokines. Here, we focused on its role as a marker of inflammation.

To investigate whether human HSCs play a role in the proinflammatory response of HCV-infected cells, JFH1-infected Huh7.5 cells were cocultured with LX2 cells, which are an HSC line generated by spontaneous immortalization in low-serum conditions (15). The expression of MIP-1β mRNA was then determined by qRT-PCR. Compared to the level in uninfected Huh7.5 cells, HCV infection induced a low level of MIP-1β expression (Fig. 1A, Huh7.5/JFH1). Moreover, MIP-1β expression